Anal. Chem. **2009,** *81,* 4752–4761

Alpha-Helical Peptide-Induced Vesicle Rupture Revealing New Insight into the Vesicle Fusion Process As Monitored *in Situ* by Quartz Crystal Microbalance-Dissipation and Reflectometry

Nam-Joon Cho,[†,‡] Guoliang Wang,[§] Malin Edvardsson,[§] Jeffrey S. Glenn,[†] Fredrik Hook,[*,§] and Curtis W. Frank[*,‡]

Division of Gastroenterology, School of Medicine, Stanford University, Stanford, California 94305, Department of Chemical Engineering, Stanford University, Stanford, California 94305, and Division of Biological Physics, Chalmers University of Technology, Gothenburg, Sweden

Downloaded via NANYANG TECHNOLOGICAL UNIV on April 10, 2019 at 08:37:22 (UTC).
See https://pubs.acs.org/sharingguidelines for options on how to legitimately share published articles.

We have used simultaneous quartz crystal microbalance-dissipation (QCM-D) monitoring and four-detector optical reflectometry to monitor *in situ* the structural transformation of intact vesicles to a lipid bilayer on a gold surface. The structural transformation of lipid vesicles to a bilayer was achieved by introducing a particular amphiphathic, α-helical (AH) peptide. The combined experimental apparatus allows us to simultaneously follow the acoustic and optical property changes of the vesicle rupturing process upon interaction with AH peptides. While QCM-D and reflectometry have similar sensitivities in terms of mass and thickness resolution, there are unique advantages in operating these techniques simultaneously on the same substrate. These advantages permit us to (1) follow the complex interaction between AH peptides and intact vesicles with both acoustic and optical mass measurements, (2) calculate the amount of dynamically coupled water during the interaction between AH peptides and intact vesicles, (3) demonstrate that the unexpectedly large increase of both adsorbed mass and the film's energy dissipation is mainly caused by swelling of the vesicles during the binding interaction with AH peptides, and (4) permit us to understand the structural transformation from intact vesicles to a bilayer via the AH peptide interaction by monitoring viscoelastic properties, acoustic mass, optical mass, and thickness changes of both the binding and destabilization processes. From the deduced "hydration signature" we followed the complex transformation of lipid assemblies. On the basis of this information, a mechanism of this structural transformation is proposed that provides new insight into the process of vesicle fusion on solid substrates.

The quartz crystal microbalance-dissipation (QCM-D) technique has been shown to be highly sensitive to the mass changes and to the viscoelastic properties of an adlayer.[1−5] It has been widely utilized in nanorange mass detection due to its high sensitivity, reliability, and simplicity. It is also a popular instrument for *in situ* measurements of biomacromolecular interactions in liquid-state research applications.[2−6] Finally, it has been proven to be a valuable technique for studying interactions between biomacromolecules at liquid−solid interfaces including protein−lipid bilayer,[7−12] cell−cell[13,14] and antibody−antigen interactions,[7−12] as well as biological signal transduction processes[15,16] and biomolecule detection.[17−19]

While QCM-D is an acoustic-based sensor, reflectometry is an optical detection technique that probes the effective thickness and effective refractive index of thin films adsorbed on a solid surface, making it a highly sensitive tool for monitoring interfacial

* To whom correspondence should be addressed. Professor Fredrik Hook, e-mail fredrik.hook@chalmers.se; Professor Curtis W. Frank, e-mail curt.frank@stanford.edu.

[†] Division of Gastroenterology, School of Medicine, Stanford University.

[‡] Department of Chemical Engineering, Stanford University.

[§] Division of Biological Physics, Chalmers University of Technology.

(1) Hook, F.; Rodahl, M.; Kasemo, B.; Brzezinski, P. *Proc. Natl. Acad. Sci. U.S.A.* **1998**, *95*, 12271–12276.
(2) Cho, N. J.; Cho, S. J.; Cheong, K. H.; Glenn, J. S.; Frank, C. W. *J. Am. Chem. Soc.* **2007**, *129*, 10050–10051.
(3) Cho, N. J.; Kanazawa, K. K.; Glenn, J. S.; Frank, C. W. *Anal. Chem.* **2007**, *79*, 7027–7035.
(4) Keller, C. A.; Glasmastar, K.; Zhdanov, V. P.; Kasemo, B. *Phys. Rev. Lett.* **2000**, *84*, 5443–5446.
(5) Keller, C. A.; Kasemo, B. *Biophys. J.* **1998**, *75*, 1397–1402.
(6) Cho, N. J.; Cheong, K. H.; Lee, C.; Frank, C. W.; Glenn, J. S. *J. Virol.* **2007**, *81*, 6682–6689.
(7) Ohtsuka, K.; Kajiki, R.; Waki, M.; Nojima, T.; Takenaka, S. *Analyst* **2004**, *129*, 888–889.
(8) Mascini, M.; Macagnano, A.; Monti, D.; Del Carlo, M.; Paolesse, R.; Chen, B.; Warner, P.; D'Amico, A.; Di Natale, C.; Compagnone, D. *Biosens. Bioelectron.* **2004**, *20*, 1203–1210.
(9) Li, J.; Thielemann, C.; Reuning, U.; Johannsmann, D. *Biosens. Bioelectron.* **2005**, *20*, 1333–1340.
(10) Hianik, T.; Ostatna, V.; Zajacova, Z.; Stoikova, E.; Evtugyn, G. *Bioorg. Med. Chem. Lett.* **2005**, *15*, 291–295.
(11) Wang, Z.; Zhang, L.; Lu, J. *J. Mol. Model. (Online)* **2005**, *11*, 80–86.
(12) Ersoz, A.; Denizli, A.; Ozcan, A.; Say, R. *Biosens. Bioelectron.* **2005**, *20*, 2197–2202.
(13) Redepenning, J.; Schlesinger, T. K.; Mechalke, E. J.; Puleo, D. A.; Bizios, R. *Anal. Chem.* **1993**, *65*, 3378–3381.
(14) Gryte, D. M.; Ward, M. D.; Hu, W. S. *Biotechnol. Prog.* **1993**, *9*, 105–108.
(15) Fung, Y. S.; Wong, Y. Y. *Anal. Chem.* **2001**, *73*, 5302–5309.
(16) Li, J.; Wu, Z. Y.; Xiao, L. T.; Zeng, G. M.; Huang, G. H.; Shen, G. L.; Yu, R. Q. *Anal. Sci.* **2002**, *18*, 403–407.
(17) Marx, K. A. *Biomacromolecules* **2003**, *4*, 1099–1120.
(18) Sota, H.; Yoshimine, H.; Whittier, R. F.; Gotoh, M.; Shinohara, Y.; Hasegawa, Y.; Okahata, Y. *Anal. Chem.* **2002**, *74*, 3592–3598.
(19) Marx, K. A.; Zhou, T.; Montrone, A.; Schulze, H.; Braunhut, S. J. *Biosens. Bioelectron.* **2001**, *16*, 773–782.

10.1021/ac900242s CCC: $40.75 © 2009 American Chemical Society
Published on Web 05/21/2009

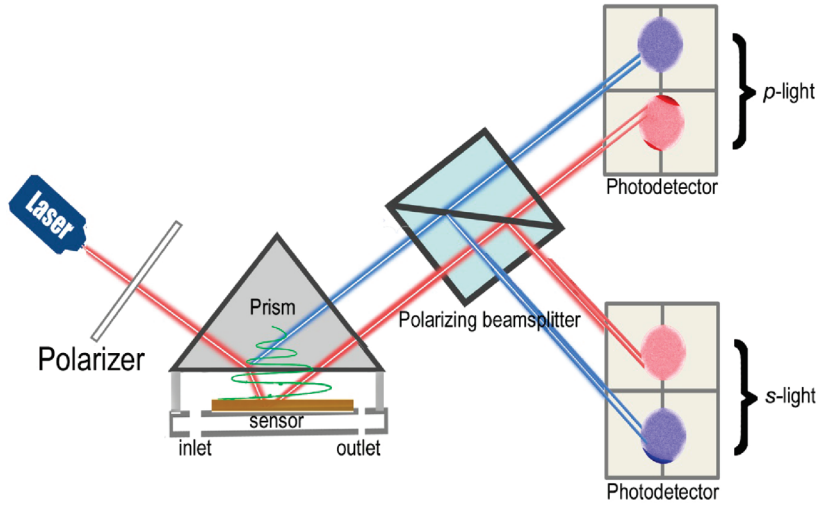

Figure 1. Visual representation of the combined quartz crystal microbalance-dissipation and reflectometry setup. The red line represents conventional reflectometry. The modified reflectometry setup is able to detect reflection of additional beams to correct distortion arising from conventional reflectometry, as shown in the blue line.

phenomena.[20,21] In recent years, reflectometry has become widely used to characterize soft, biological films and to monitor binding events due to its high degree of sensitivity, label-free analyte binding detection, and ability to resolve the kinetics of biomacromolecular interactions in real time. In our apparatus,[22] a reflected beam is generated by coupling plane-polarized light obliquely to the liquid−solid interface by a polarizing beamsplitter. The intensities of the parallel (I_p) and the perpendicular (I_s) components are monitored, and the output signal is defined as their ratio $S = I_p/I_s$. The change in the ratio S is related to the change in the effective thickness and/or the effective refractive index of the adsorbed layer. In addition, to overcome errors arising from the prism−bulk solution interface of conventional reflectometry measurements, the distorted signal is corrected by adding an additional beam, as shown in Figure 1 (dashed line, see also ref 22 and references therein).

Despite the widespread use of optical-based techniques,[23−27] there are inherent limitations in measurements based on a single quantity. In order to overcome these barriers, researchers have attempted to use combined techniques[22,28−32] that use different physical principles to monitor biological phenomena. As biological model systems become more complex, there is increasing need to simultaneously measure several independent physical parameters in order to correctly and precisely interpret biological phenomena.

By using QCM-D and reflectometry simultaneously to monitor interfacial phenomena, we are able to analyze the dynamics of multistep processes by combining two measurements that rely on fundamentally different physical principles.[22] Furthermore, flawed assumptions intrinsic to data analysis become clear, and differences arising from use of different techniques can often be resolved through theoretical representations.

The model system depicted here is based on our previous studies[2,3] in which we demonstrated that an amphiphathic, α-helical (AH) peptide can be used as a destabilizing agent to rupture intact adsorbed vesicles, leading to lipid bilayer formation on a gold substrate. The AH peptide is known to be a necessary linker for membrane association of the hepatitis C virus (HCV) NS5A protein, which is required for viral replication.[6,33] The secondary structure of the AH peptide estimated from a set of prediction methods provides structural information about the AH peptide's conformational shape, as seen in Figure 2. Furthermore, circular dichroism (CD) confirmed the α-helical secondary structure of the AH peptide, as indicated by the minima at 208 and 222 nm depicted in Figure 2b.

Classical vesicle fusion kinetics on hydrophilic substrates such as mica, glass, and silicon oxide follow a two-step process.[5] Vesicles first adsorb on the substrate up to a particular, incomplete saturation point that varies depending on physical parameters including osmotic pressure, vesicle size, temperature, substrate composition, and pH.[2,3,5,34] Then, the adsorbed vesicles rupture and form a supported bilayer due to a so-far-not-fully understood combination of vesicle-vesicle and, most importantly, vesicle−substrate interactions. By contrast, the model system presented in this paper involves complete saturation of intact vesicles adsorbed on a gold substrate, followed by a structural transforma-

(20) Majewski, J.; Kuhl, T. L.; Wong, J. Y.; Smith, G. S. *J. Biotechnol.* **2000**, *74*, 207–231.
(21) Knoll, W. *Annu. Rev. Phys. Chem.* **1998**, *49*, 569–638.
(22) Wang, G.; Rodahl, M.; Edvardsson, M.; Svedhem, S.; Ohlsson, G.; Hook, F.; Kasemo, B. *Rev. Sci. Instrum.* **2008**, *79*, 075107.
(23) Ekgasit, S.; Thammacharoen, C.; Knoll, W. *Anal. Chem.* **2004**, *76*, 561–568.
(24) Ekgasit, S.; Yu, F.; Knoll, W. *Langmuir* **2005**, *21*, 4077–4082.
(25) Yu, F.; Yao, D.; Knoll, W. *Anal. Chem.* **2003**, *75*, 2610–2617.
(26) Voros, J.; Ramsden, J. J.; Csucs, G.; Szendro, I.; De Paul, S. M.; Textor, M.; Spencer, N. D. *Biomaterials* **2002**, *23*, 3699–3710.
(27) Stroumpoulis, D.; Parra, A.; Tirrell, M. *AIChE J.* **2006**, *52*, 2931–2937.
(28) Bailey, L. E.; Kambhampati, D.; Kanazawa, K. K.; Knoll, W.; Frank, C. W. *Langmuir* **2002**, *18*, 479–489.
(29) Hook, F.; Kasemo, B.; Nylander, T.; Fant, C.; Sott, K.; Elwing, H. *Anal. Chem.* **2001**, *73*, 5796–5804.
(30) Reimhult, E.; Larsson, C.; Kasemo, B.; Hook, F. *Anal. Chem.* **2004**, *76*, 7211–7220.
(31) Richter, R.; Mukhopadhyay, A.; Brisson, A. *Biophys. J.* **2003**, *85*, 3035–3047.
(32) Richter, R. P.; Brisson, A. R. *Biophys. J.* **2005**, *88*, 3422–3433.
(33) Elazar, M.; Cheong, K. H.; Liu, P.; Greenberg, H. B.; Rice, C. M.; Glenn, J. S. *J. Virol.* **2003**, *77*, 6055–6061.
(34) Reimhult, E.; Hook, F.; Kasemo, B. *Phys. Rev. E: Stat., Nonlinear, Soft Matter Phys.* **2002**, *66*, 051905.

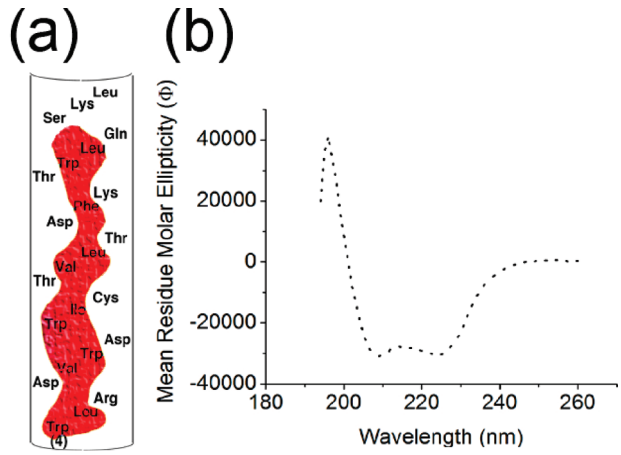

Figure 2. N-terminal amino acid sequence of amphipathic helix (AH) derived from nonstructural 5A(NS5A) protein. (a) The AH peptide of the hepatitis C virus (HCV) nonstructural protein NS5A with sequences SGSWLRDVWDWICTVLTDFKTWLQSKL is conserved across HCV isolates. The amphipathic nature of the helix (indicated by the red hydrophobic continuous band in side view) is also conserved. (b) The CD spectrum (AH peptide) displays double peaks at 209 and 222 nm, corresponding to an α-helical secondary structure. (c) Protein secondary structures were deduced from the set of prediction methods available at the NPSA Web site, including DSC, HNNC, MLRC, PHD, SOPM and Sec. Cons., and demonstrate that the AH peptide has an α-helical nature.

tion of the vesicle monolayer to a lipid bilayer that is caused by AH peptide−vesicle interactions.

In our previous studies,[2,3] we distinguished the properties of this structural transformation using different viscoelastic models and sought to explain the structural transformation with the antimicrobial peptide mode of action. During the initial binding of AH peptide, we observed large frequency and dissipation changes. It was hypothesized that AH peptides first created instability of the vesicle surface following binding. This may lead to expansion of the vesicles as well as create innumerable fingerlike structures[35,36] on the outer leaflet of the vesicles. These structural changes are reasonable explanations for both the large changes in frequency due to the presumed expansion of vesicles (increase in bound water) as well as the increase in dissipation attributable to both vesicle expansion and development of microvilli structure.

To *quantitatively* analyze this transformation, we employed in this work a combined QCM-D and reflectometry setup,[22] allowing us to separate the acoustic mass, m_a, calculated from QCM-D data, and the optical mass, m_o, calculated from reflectometry data, providing information about the change in solvent mass during the structural transformation from intact vesicles to a bilayer on a gold substrate. To characterize this process, we define the hydration signature, which can only be calculated by simultaneously measuring optical and acoustic mass changes; this allows distinct phases in the rupture process to be distinguished and quantified. Further, the resulting bilayer is complete, as evidenced by QCM-D and reflectometry data, and is in excellent agreement with lipid bilayers formed via the vesicle fusion process in the absence of peptides.[30−32,4,5]

OVERVIEW OF RELEVANT THEORY

Quartz Crystal Microbalance-Dissipation and Reflectometry. A wealth of information regarding QCM-D principles and modeling has been published by many research groups, including our own.[37−41,3] A widely accepted merit of the QCM-D technique is its ability to detect an adsorbed mass, Δm, deposited onto a thin rigid quartz surface. To a first approximation, the added mass and the change in resonant frequency are governed by a linear relationship, as described by Sauerbrey.[42] If the adlayer is rigid enough (energy dissipation, $\Delta D < 1 \times 10^{-6}$), one can use the Sauerbrey equation to obtain the mass, $\Delta m_{\text{Sauerbrey}}$, of the adsorbate with the assumption that the adsorbed mass is homogeneous with a spatially uniform density, as follows:

$$\Delta m_{\text{Sauerbrey}} = C_{\text{QCM}} \frac{\Delta f_z}{z} \qquad (1)$$

where Δm is the adsorbed mass on the surface, C_{QCM} is the mass sensitivity constant (-17.7 ng cm^{-2} Hz^{-1} for an AT-cut quartz crystal with $f = 5$ MHz) and Δf_z is the change in the resonant frequency at the zth harmonic ($z = 1,3,5\ldots$).

In addition to sensitive detection of an adsorbed mass, the QCM-D apparatus can also detect the mechanical properties of the adlayer by measuring the energy dissipation due to frictional losses associated with molecular interactions. For the viscoelastic regime of a "soft" layer with high energy dissipation, the Sauerbrey relationship is not valid. In such cases, the effects of the layer on the resonant frequency and dissipation are better represented by mechanical elements coupled to a rigid quartz layer. This can be done in two ways. The Maxwell approach treats the coupling as a series combination of a spring and a dash pot. The Voigt approach treats the coupling as a parallel combination of a spring and dash pot.[3] This second mechanical model has been used in the Voigt−Voinova analysis. In this case, the adsorbed layer is represented with an effective thickness, d_{eff}, an effective density, ρ_{eff}, an effective shear elasticity, μ_{eff}, and an effective shear viscosity, η_{eff}. The Voigt−Voinova model includes these viscoelastic effects and assumes a liquid with Newtonian characteristics, uniform thickness, uniform film density, and no slip.

(35) Gidalevitz, D.; Ishitsuka, Y.; Muresan, A. S.; Konovalov, O.; Waring, A. J.; Lehrer, R. I.; Lee, K. Y. *Proc. Natl. Acad. Sci. U.S.A.* **2003**, *100*, 6302–6307.
(36) Mecke, A.; Lee, D. K.; Ramamoorthy, A.; Orr, B. G.; Banaszak Holl, M. M. *Biophys. J.* **2005**, *89*, 4043–4050.
(37) Kanazawa, K. K. *J. Electroanal. Chem.* **2002**, *524*, 103–109.
(38) Kanazawa, K. K.; Reed, C. E. *Abstr. Pap. Am. Chem. Soc.* **1989**, *198*, 89-Anyl.
(39) Rodahl, M.; Hook, F.; Kasemo, B. *Anal. Chem.* **1996**, *68*, 2219–2227.
(40) Rodahl, M.; Hook, F.; Krozer, A.; Brzezinski, P.; Kasemo, B. *Rev. Sci. Instrum.* **1995**, *66*, 3924–3930.
(41) Rodahl, M.; Kasemo, B. *Sens. Actuators, B: Chem.* **1996**, *37*, 111–116.
(42) Sauerbrey, G. *Z. Phys.* **1959**, *155*, 206–222.

Furthermore, it is assumed that the film viscosity is independent of frequency overtone. Then, the changes in the resonant frequency, Δf, and dissipation, ΔD, can be expressed in terms of the film density, viscoelastic properties, and thickness by a Taylor expansion:[3]

$$\Delta f \cong \frac{1}{2\pi\rho_q t_q} t_f \rho_f \omega \left(1 + \frac{2t^2\chi}{3\delta^2(1+\chi^2)}\right) \quad (2)$$

$$\Delta D \cong \frac{2t^3\rho_f f}{3\pi f_{ro}\rho_q t_q} \frac{1}{\delta^2(1+\chi^2)} \quad (3)$$

where ρ_q and ρ_f are the density of the quartz and film, respectively; t_q and t_f are the thickness of the quartz and film, respectively; f is the measured frequency; χ is the ratio of the storage modulus, μ, and the loss modulus, η, which is the inverse of tan δ.

The mass uptake can then be deduced as follows:

$$m_a = \rho_{eff} d_{eff} \quad (4)$$

The calculated acoustic mass, m_a, includes solvent that surrounds the adsorbed materials or is hydrodynamically coupled to the adsorbing film (e.g., in interstitial spaces between intact vesicles or within the vesicles). The acoustic mass is a combination of optical mass, m_o, and solvent mass, m_s, such that

$$m_a = m_o + m_s \quad (5)$$

Typically, the optical mass can be obtained by using Feijter's formula[43] as follows:

$$m_o = \frac{d_{eff}(n - n_0)}{(dn/dc)} \quad (6)$$

where n is the effective refractive index of the adlayer, n_0 is the refractive index of the ambient medium, and dn/dc is the refractive index increment of the adsorbed molecules. In many cases, accurate bulk values of dn/dc are hard to measure or do not represent the molecules in the adsorbed state, which is especially true in cases where surface-induced structural changes occur. In such cases, the Lorenz−Lorentz formula provides an alternative route to more accurately calculate the mass of the adlayer:[44]

$$m_o = d_{eff}(n - n_0) \frac{3(n + n_0)}{(n^2+2)\{r(n_0^2+2) - v(n_0^2-1)\}} \quad (7)$$

where r and v are the specific refractivity and the partial specific volume of the adlayer, respectively. It is evident that d_{eff} and n must be known explicitly to determine the optical mass. Under the assumption that QCM-D and reflectometry sense the same effective thickness, d_{eff}, detected masses are governed by[45]

$$\frac{m_a}{\rho_{eff}} = \frac{m_o}{\rho} + \frac{m_a - m_o}{\rho_s} \quad (8)$$

The optical mass of the adlayer can be found by substituting eq 7 into eq 8, provided that the effective refractive index, n, satisfies the equation:[22,30,45]

$$n^3 + (Q - n_0 - V)n^2 + 2n - (2n_0 + 2V + Qn_0^2) = 0 \quad (9)$$

where

$$V = \frac{1}{A}\frac{S - S_0}{S_0}\frac{\rho_s}{m_a} \quad (10a)$$

$$Q = \frac{1}{m_a}\frac{\rho_s - \rho}{\rho}\frac{3}{r(n_0^2+2) - v(n_0^2-1)}\frac{1}{A}\frac{S - S_0}{S_0} \quad (10b)$$

From the calculated solvent mass and acoustic mass, we can derive the hydration parameter of the layer, H, as follows:

$$H = \frac{m_s}{m_a} \quad (11)$$

The hydration signature will add valuable information to follow complex biological interaction processes.

MATERIALS AND METHODS

Small Unilamellar Vesicle and Substrates. Small unilamellar vesicles of 1-palmitoyl-2-oleoyl-*sn*-glycero-3-phosphocholine (POPC) (Avanti Polar Lipids, Alabaster) were prepared by the extrusion method. For QCM-D and reflectometry measurements, we used a PBS buffer, 10 mM PBS (pH 7.5), and 200 mM NaCl solution in 18.2 MΩ cm Milli-Q water (MilliPore, Oregon). Extruded unilamellar vesicles (referred to simply as vesicles) were prepared in the following manner. Lipid films were prepared by first drying the as-supplied lipids dissolved in chloroform under a gentle stream of nitrogen at room temperature. The resulting lipid film was then stored under vacuum overnight to remove residual chloroform. Multilamellar vesicles were prepared by swelling the lipid film in an aqueous solution, then vortexing periodically for 5 min. The resulting multilamellar vesicles were extruded by a Mini Extruder (Avanti Polar Lipids, Alabaster) through polycarbonate membranes with 50 nm pores and then again with 30 nm pores. The resulting average diameter of vesicles was 61 ± 2.1 nm. Vesicles were prepared at a nominal lipid concentration of ∼5 mg mL^{-1} for QCM-D and reflectometry experiments, then subsequently diluted before experiments. Vesicles were generally used within 3 days of preparation. The peptide concentration used for the combined QCM-D and reflectometry experiments was 20 μM.

Silicon oxide- and gold-coated quartz crystal sensors were obtained from Q-Sense (Q-Sense AB, Gothenburg, Sweden). Prior to use, the substrates were soaked in a 10 mM sodium dodecyl sulfate (SDS) solution for 30 min, then rinsed with water and ethanol, respectively. After drying with a stream of nitrogen air, the crystals were placed in a custom-built UV/ozone chamber for at least 120 min.

(43) Feijter, J. A. D.; Benjamins, J.; Veer, F. A. *Biopolymers* **1977**, *17*, 1759–1772.
(44) Cuypers, P. A.; Corsel, J. W.; Janssen, M. P.; Kop, J. M.; Hermens, W. T.; Hemker, H. C. *J. Biol. Chem.* **1983**, *258*, 2426–2431.
(45) Larsson, C.; Rodahl, M.; Hook, F. *Anal. Chem.* **2003**, *75*, 5080–5087.

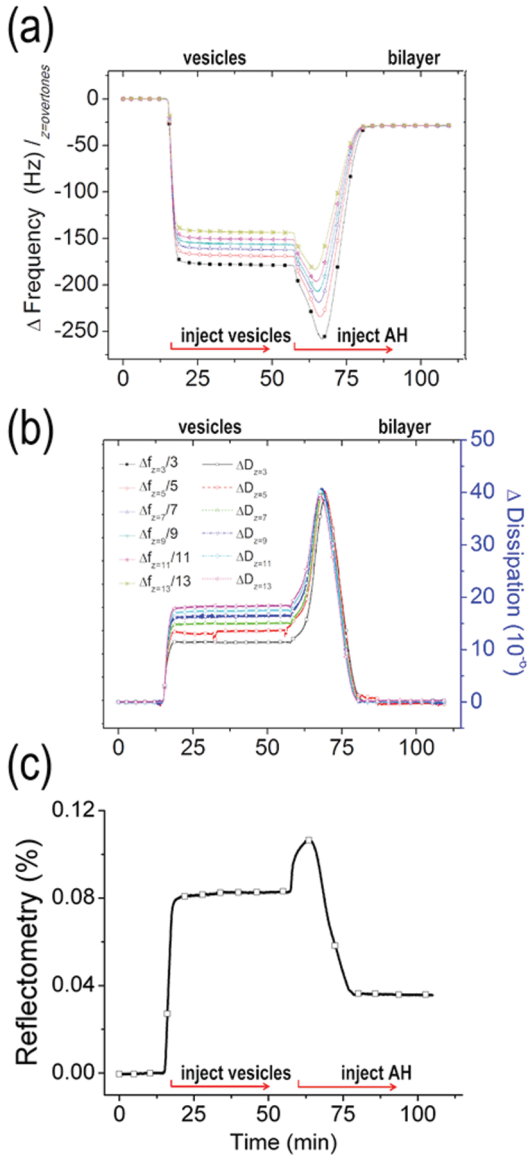

Figure 3. Combined QCM-D and reflectometry responses for structural transformation from intact vesicles to a bilayer induced by the AH peptide. (a) QCM-D data of $\Delta f_{z=\text{overtones}}/z$ as a function of time depicting the vesicle adsorption process with PBS buffer solution (200 mM NaCl, pH 7.53). We display the overtones, z, up to the 13th. Vesicles are added after stabilizing the frequency signal for 15 min. Upon the addition of the AH peptide, a huge uptake of mass can be observed, followed by the formation of a bilayer on the gold substrate. Throughout the experiments, we used laminar flow conditions. (b) The corresponding energy dissipation versus time plot demonstrates that the viscoelastic nature of the film changes during the structural transformation from intact vesicles to a complete, rigid bilayer. (c) Simultaneously, the reflectometric response was also obtained.

Peptides. An amphipathic α-helical (AH) peptide was synthesized by Anaspec Corporation (San Jose, CA). The sequence of the AH peptide is H-Ser-Gly-Ser-Trp-Leu-Arg-Asp-Val-Trp-Asp-Trp-Ile-Cys-Thr-Val-Leu-Thr-Asp-Phe-Lys-Thr-Trp-Leu-Gln-Ser-Lys-Leu-Asp-Tyr-Lys-Asp-NH_2. In addition, protein secondary structures were deduced from a large set of prediction methods available at the NPSA Web site, including DSC, HNNC, MLRC, PHD, SOPM and Sec. Cons (see http://npsa-pbil.ibcp.fr/NPSA and references therein). Further, CD spectra were recorded on an Aviv model 215 spectrometer equipped with a 450 W Xenon arc lamp light source, a double-fused silica prism monochromator with a range of 165−1200 nm, and a MgF_2 polarizer, calibrated with ammonium *d*-10-camphorsulfonate. Routinely, measurements were done at 25 °C in 0.1 cm path-length quartz FUV-grade rectangular cuvettes (Hellma) with protein concentrations ranging from 0.01 to 0.03 mM in a 10 mM Tris buffer (pH 7.4, 10 mM Tris-HCl). Spectral scans were recorded in the 190−270 nm wavelength range with 1.0 nm increments and 2 s integration times and averaged over three scans. The baseline-corrected spectra were smoothed by using a third-order least-squares polynomial fit. Scans were corrected for background noise, based on blanks of PBS buffer, and the obtained scans in ellipticity (θ) were converted to mean molar residue ellipticity ($[\theta]$).

Dynamic Light Scattering. Dynamic light scattering (DLS) was performed on a 90Plus Particle Size Analyzer and results were analyzed by digital autocorrelator software (Brookhaven Instruments Corporation, New York). All measurements were taken at a scattering angle of 90° where the reflection effect is minimized. All autocorrelation functions obtained were also analyzed by CONTIN and non-negatively constrained least squares (NNLS) algorithms to check for multimodal distributions.

Combined Quartz Crystal Microbalance-Dissipation and Four-Detector Reflectometry. The combined QCM-D and reflectometry setup was provided by Q-Sense AB (Q-Sense AB, Gothenburg, Sweden). Detailed description of the setup can be found in ref 22. In brief, a custom-built titanium flow chamber was used to accommodate the quartz crystal. The volume of the void adjacent to the sensor crystal is approximately 90 μL, and the chamber was designed to provide laminar flow with minimum signal distortion. A laser diode (λ = 635 nm) is polarized by a linear polarizer and coupled to the solid substrate through a right-angle prism. The two outgoing beams are divided into p- and s-polarized light with a polarizing beam splitter. The intensities, I_p and I_s, of the reflected beams are monitored by four photodiodes in order to correct for the noise to the reflectometric unexpected signal arising from adsorption at the prism−bulk solution interface. Using three different overtones, we fit changes in the frequency and dissipation to the film effective density, ρ_{eff}, effective shear elasticity, μ_{eff}, effective shear viscosity, η_{eff}, and a thickness, t_{eff}. Overtones were fitted to this model using the commercial software program, Q-Tools (Q-Sense AB). Note that usually either ρ_{eff} or t_{eff} is required as a known input in the models.

RESULTS

Simultaneous QCM-D and Reflectometry Measurements to Follow the Transformation from Intact Vesicles to the Bilayer. Characteristic results from QCM-D measurements of intact vesicle adsorption on a gold substrate followed by the addition of AH peptide are shown in parts a and b of Figure 3. The simultaneously measured reflectometry signal is presented in Figure 3c. Changes in frequency, $\Delta f_z/z$, and energy dissipation, ΔD_z, obtained at six different overtones (z = 3 for the third and 5, 7, 9, 11, and 13 for subsequent overtones) are displayed as a function of time. As previously illustrated,[3] a non-Sauerbrey, viscoelastic regime can be resolved from the overtone QCM-D responses of $\Delta f_z/z$ and ΔD_z. The following two regimes were identified: (i) the intact vesicles regime, from

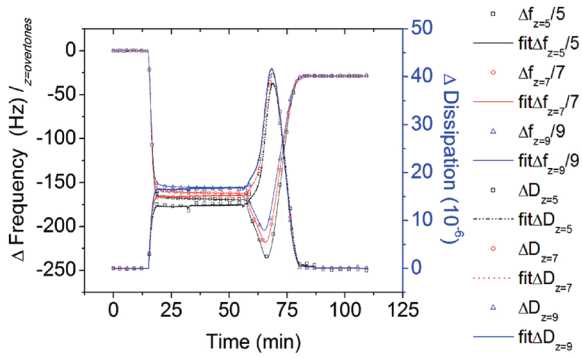

Figure 4. Model to fit experimental QCM-D data using three different overtones to the Voigt element-based viscoelastic model. We used a Voigt element-based model to fit $\Delta f_z/z$ for the structural transformation of intact vesicles to a bilayer induced by addition of the AH peptide. The fits between the viscoelastic model (Q-tool parameters of fluid density, fluid viscosity, and adlayer density were 1000 kg m^{-3}, 0.001 kg m^{-1} s^{-1}, and 1100 kg m^{-3}, respectively) and the experimental data are presented. The corresponding ΔD_z fit using the same model is also presented.

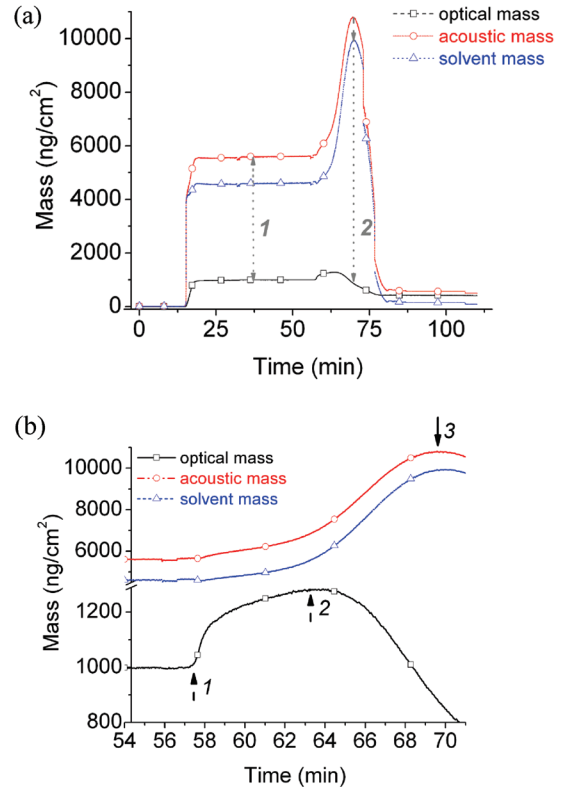

Figure 5. Determination of the solvent mass obtained by QCM-D and by reflectometry. (a) Following the time-resolved variation of structural transformation of intact vesicles to a bilayer using the acoustic mass (red long-dotted line) and the optical mass (black line) to separate out the mass contributed by the water/solvent mass (blue dot). Strikingly, the solvent mass follows the huge uptake of acoustic QCM-D mass, demonstrating that the main contribution of uptake of mass is due to swelling of the vesicles upon the initial interaction with the AH peptide. Parameters used for calculating optical mass and solvent mass were $\rho_{solvent}$ = 1.0 g m^{-3}, r = 0.286 cm^3 g, ρ = 1.02 g cm^{-3}, v = 0.98 cm^3 g^{-1}, and n_0 = 1.334. (b) Magnified view of the graph in part a. Note that there is a break on the *y*-axis from 1290 to 4500 ng/cm^{-2}, the lower and upper scales differ by a factor of ~15, and the data are only plotted from 54 to 70 min.

both $\Delta f_z/z$ and ΔD_z overtones, values deviated ~15.2% and 39.4%, respectively. The overtone deviations were a result of coupled and associated solvent within intact vesicles, which have viscoelastic properties. (ii) Rigid bilayer regime, induced by AH peptide interactions, $\Delta f_z/z$, and ΔD_z overtones merged to ~−27.4 Hz and ~0.023, respectively. The values represent a rigid, complete bilayer, whose thickness can be modeled with the Sauerbrey equation, as shown in parts a and b of Figure 3 (see eq 1). Though $\Delta f_z/z$ and ΔD_z clearly distinguished two different viscoelastic layers, the two parameters are not sufficient to resolve the intermediate stages between intact vesicles and bilayer due to limitations in the information content of acoustic measurements alone.

Figure 3c displays the simultaneous optical reflectometry measurements obtained on the very same surface. While QCM-D provides structural information, reflectometry measures a single parameter and provides a measure of the bound molecular mass, which is a function of both the effective thickness and the effective refractive index of the adlayer. However, reflectometric measurement alone cannot resolve the molecular dimension of the adlayer or the refractive index of the film. This was instead accomplished by using the electromechanical-based QCM-D measurements, which measure the acoustic mass including hydrodynamically coupled water, and provides information about the effective film thickness. Hence, by combining the two techniques with appropriate theoretical representations, we were able to calculate the adsorbed molecular mass (optical mass), adsorbed molecular mass and solvent mass (acoustic mass), effective thickness, and effective reflective index over the course of time. This is especially useful for our case where significant structural changes occur, as indicated by the two regimes identified from $\Delta f_z/z$ and ΔD_z changes induced by the initial AH peptide interaction.

First, the acoustic mass was calculated using QCM-D responses from eq 2. As described in the theory section, the effective thickness was obtained by fitting experimental values to a Voigt−Voinova based model using three different overtones, as shown in Figure 4, and the effective density was initially assumed based on the effective density of water and lipids. (See ref 3 for a detailed description of two different QCM models). Despite the complexity of the system, the Voigt−Voinova model almost perfectly fits the structural transformation from adsorbed, intact vesicles to a lipid bilayer. The calculated acoustic mass is the sum of the two components, as shown in eq 3. It is noted that there are two different methods to obtain the optical mass of adsorbed materials at liquid−solid interfaces (see eqs 4 and 5). As emphasized above, it is necessary to know the refractive index of the adsorbed molecules, and this uncertainty may lead to the incorrect interpretation of complex biological interactions. In order to avoid this uncertainty, we utilized the Lorenz−Lorentz formula and eq 6 under the assumption that QCM-D and reflectometry measure the same effective thickness to obtain the optical mass, as depicted in Figure 5. We plotted the three different masses together (optical, acoustic, and solvent) in order to have a better idea for each of the mass contributions during the course of the structural transformation. Since we postulated previously that the solvent mass change essentially follows the kinetics of the acoustic mass change during the AH peptide-induced rupture of intact adsorbed vesicles, our results demonstrate that the large mass increase during the initial AH peptide interaction is mainly due to swelling of the intact vesicles.

In detail, there are four different interesting regimes to focus on (1) the adsorbed, intact vesicles regime, (2) the initial AH peptide interaction regime, (3) the vesicle rupture regime, and (4) the complete, rigid bilayer regime. First, when vesicles are adsorbed onto particular solid substrates such as gold, the vesicles' interaction with the substrate does not have sufficient energy to cause them to rupture. Instead, the interaction causes the vesicles to adsorb onto the substrate in a stable manner, forming a monolayer of ordered more-or-less spherical entities. Also, note that the kinetics for adsorption kinetics of vesicles onto a gold substrate depend on many conditions including vesicle size, concentration, temperature, pH, and flow conditions (e.g., batch or flow system).[34,46] Since the acoustic mass is the sum of the biomolecular mass (lipid ~500 ng cm^{-2}) and hydrodynamically coupled solvent (direct hydration, coupling between vesicles, encapsulation, or entrapment on a roughened surface ~3530 ng cm^{-2}), there are huge deviations between the acoustic and optical masses, as shown in Figure 5a (gray arrow 1). Interesting results were found upon addition of the AH peptide, as shown in parts a and b of Figure 5 (magnified view). From the acoustic mass derived from the QCM-D data, it is hard to distinguish the regime involving initial binding of the AH peptide, signaling minor structural changes at this stage. By contrast, the optical mass, which is less sensitive to structural changes, was able to resolve initial binding of the AH peptide (arrow 1, Figure 5b) at 57.5 min. On the basis of reflectometry measurements, saturation of AH peptide binding occurred (arrow 2, Figure 5b) at 63.3 min. At this point in time, the acoustic mass uptake attributed to the swelling of vesicles accelerates until saturation is reached at 69.4 min, while the optical mass decreased monotonically due to desorption of lipids and AH peptide mass (arrow 3, Figure 5b). The subsequent acoustic mass loss (arrow 3, Figure 5b) corresponds to the structural reorganization of lipid vesicles to form a bilayer on the gold substrate. The saturating values for optical, acoustic, and solvent masses were ~400 ng cm^{-2}, 500 ng cm^{-2}, and 90 ng cm^{-2}, respectively, all in excellent agreement with masses reported in the literature for supported lipid bilayers.[30]

Comparison of Two Hydration Signatures for Alternative Methods to Form a Supported Lipid Bilayer. Utilizing optical, acoustic, and solvent mass changes over time, we were able to extract the hydration signature, which traces the presence of bound solvent during the structural transformation process of vesicles, as shown in eq 8. In order to examine the utility of the hydration signature to describe the transformation processes, two different structural transformations of vesicles to bilayer were plotted. The first interaction is due to vesicle interaction with a hydrophilic solid substrate (e.g., SiO_x), and the other is mediated by the interaction between intact vesicles adsorbed on a gold substrate and AH peptide, as shown in Figure 6. Vesicle fusion on hydrophilic substrates such as silica, glass, and mica is well characterized.[4,5,31,32] Although the vesicle fusion process appears to be simple, determining what specific interactions dominate this process has been difficult to quantitatively analyze, and therefore, the vesicle fusion mechanism is still speculative.[27,47]

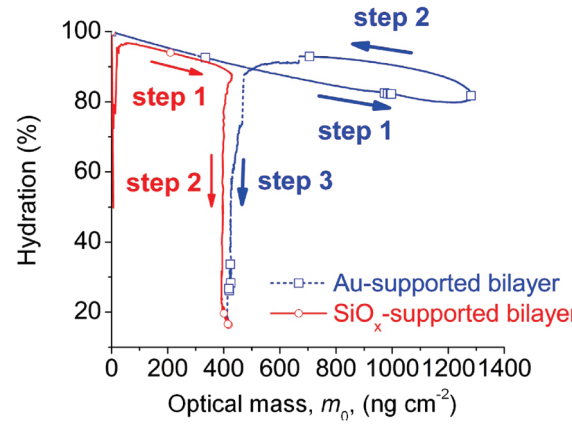

Figure 6. Hydration signatures of vesicle rupture on gold and SiO_x substrates. Dependence of film hydration (in percentage of the acoustic mass) on the optical mass for the formation of a lipid bilayer on the gold and silica surface.

The driving force of vesicle rupture is likely a combination of vesicle−substrate interactions and lateral vesicle−vesicle interactions. With the use of the hydration signature, it is possible to capture the sudden variation from vesicle to bilayer formation, which is consistent with the previously proposed scenario.[4,5] In order to fuse vesicles on a hydrophilic substrate, it is necessary for the substrate to have a critical vesicle concentration in order to promote vesicle−vesicle interactions. The hydration signature plateaus at ~90% when the critical vesicle concentration is reached, as shown in Figure 6 (red step 1). At this plateau, the optical mass has increased to ~400 ng cm^{-2}, which corresponds to the total lipid mass. Upon reaching the critical concentration, vesicles rupture to form a bilayer in an autocatalytic fashion that is mainly governed by vesicle−vesicle and favorable vesicle−substrate interactions and only minor changes in the total lipid mass. The expected acoustic mass loss is captured by QCM-D, yet during the formation of the bilayer, optical mass increases while there is a sudden decrease in hydration signature (red step 2). This rapid decrease is due to structural transformation, resulting in bilayer formation. When taken in the context of the acoustic and optical mass data, it is seen that the hydration signature can be used as an excellent indicator of viscoelastic properties of the adlayer and is in excellent agreement with previous work addressing the mechanical properties of this system in detail.[3]

Contrary to the situation for the silicon oxide substrate, as vesicles first adsorbed on the gold substrate, the hydration signature decreased and reached a plateau around 80% (blue step 1). It is worth noting that the relative decrease in hydration versus optical mass is identical for both substrates (~1% per 50 ng cm^{-2}) even though the optical mass associated with the critical coverage prior to rupture (~400 ng cm^{-2}) on the silicon oxide substrate is more than 2 times less than the intact vesicle monolayer on the gold substrate (~1000 ng cm^{-2}) and 3 times less than the lipid plus peptide mass (~1300 ng cm^{-2}). The lipid mass at saturated coverage is in good agreement with a vesicle coverage corresponding to the jamming limit of 54% upon irreversible random sequential adsorption, and the critical vesicle coverage on SiO_x corresponds to ~20%, in good agreement with previous results if also the high vesicle deformation on SiO_x is taken into account.[30] The relatively high

(46) Reimhult, E.; Zach, M.; Hook, F.; Kasemo, B. *Langmuir* **2006**, *22*, 3313–3319.
(47) Johnson, J. M.; Ha, T.; Chu, S.; Boxer, S. G. *Biophys. J.* **2002**, *83*, 3371–3379.

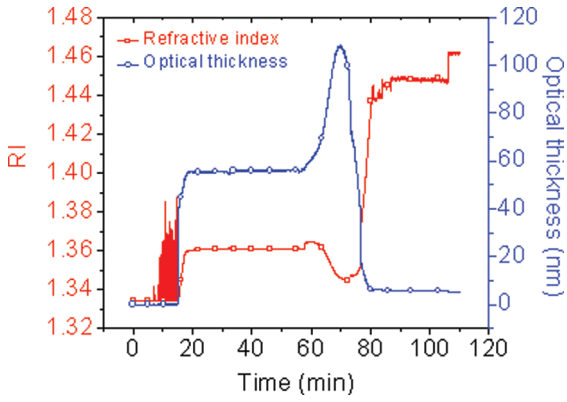

Figure 7. Time-resolved refractive index (−□−) and optical thickness (−○−) of the lipid bilayer formation on gold substrates.

hydration (~80%) observed here is consistent with previous results, indicating that the major contribution to the acoustic mass increase is from solvent in the interstices of the monolayer of intact vesicles and inside vesicles. Strikingly, upon addition of AH peptide, the total mass increases by approximately 30% prior to vesicle rupture, while the hydration rapidly increases (blue step 2), consistent with swelling of vesicles induced by the AH peptide followed by a decrease in the optical mass due to desorption of AH peptides and lipids. Note, however, that although lipid and AH peptide mass loss must occur to explain the large reduction in optical mass, the level of hydration remains higher than upon vesicle adsorption, until there is a sharp decrease in hydration upon vesicle rupture and subsequent bilayer formation (blue step 3). This huge drop of hydration from ~90% to 20% was accompanied by a significant increase in viscosity and a decrease in the shear modulus of the film, supporting the structural transformation from "soft" vesicles (due to hydrodynamically coupled solvent) to a "rigid" bilayer.

In addition to the estimate of solvent mass from acoustic mass, the formalism used made it possible to obtain the time-dependent variation in optical thickness and reflective index, as shown in Figure 7. The obtained thickness (~5.1 nm) and effective refractive index (~1.45) of the complete bilayer are in very good agreement with expectations,[30] although not easily obtained via other techniques. Similarly, an optical thickness of around 50 nm is consistent with a monolayer of slightly deformed lipid vesicles, whose average size in suspension was 61 nm. Note, in particular, that there is a significant reduction in effective film refractive index that is accompanied by an almost 2-fold increase in thickness upon vesicle swelling. Interestingly, the largest nearest neighbor distance for randomly adsorbed lipid vesicles (see above) corresponds to the vesicle diameter, while a substantial amount of vesicles are located significantly closer to each other. Hence, an increase in effective thickness by a factor of 2 upon swelling suggests that not only swelling but also lateral vesicle−vesicle interactions are required for peptide-induced bilayer formation.

DISCUSSION

Vesicle Swelling Caused by AH Peptide. Previously, we reported that, upon initial interaction with AH peptide, there is a characteristic QCM-D signal response characterized by significant changes in frequency and dissipation.[2,3] Upon electrostatic interaction with an intact vesicle, AH peptides may create a physical instability on the outer bilayer leaflet. This may lead to swelling of the vesicles (local osmotic pressure) and/or the creation of microvilli (fingerlike structures) on the vesicles. These proposed effects could explain both the large decrease in frequency and increase in dissipation as the vesicles swell and their bound water content increases. Since the QCM-D response corresponds to the acoustic mass (e.g., combination of lipid and water mass) change, we integrated simultaneously measured complementary data using reflectometry in order to trace the complex biological interaction from a new angle. We found, primarily through the possibility offered to separate lipid and water mass, that this strategy reveals new insight into the vesicle fusion mechanism. First, over the course of 5 min, AH peptides start to bind to the intact vesicles (arrow 1, Figure 5b) and create a plateau (arrow 2, Figure 5b). During the initial binding of AH peptide, until 62.2 min (arrow 2, Figure 5), the solvent mass does not change significantly. This is consistent with the existence of a critical concentration of bound AH peptide at which point vesicle destabilization and swelling occur. Following the initial AH peptide binding step, the solvent mass starts to increase sharply at around 64 min, indicating that the intact vesicles swell, while the bound mass of AH peptide plateaus. Also note that during the swelling process, both AH peptide and lipid mass, presumably in the form of "budding" vesicles, desorb from the substrate. This view is clearly supported by comparing two different hydration signatures of bilayer formation. While bilayer formation on a hydrophilic, solid substrate involves a continuous loss of solvent (e.g., encapsulated water within vesicles) as vesicles rupture individually, the hydration signature of the bilayer formed by the AH peptide rupture of intact vesicles sensitively captures the increasing solvent mass as the optical mass decreases. This finding correlates well with previously proposed vesicle fusion mechanisms.[5,27,47] In the case of hydrophilic substrates such as SiO_x, attractive vesicle−substrate interactions cause individual vesicle rupture that submerges detection of the mechanistic events behind the deformation and rupturing processes. However, the process of intact vesicle rupture by AH peptide reveals an intermediate process of vesicle swelling, which provides new insight into the vesicle fusion mechanism. To our knowledge, this is the first quantitative analysis to characterize the vesicle swelling process mediated by AH peptide, providing a mechanistic model as described below.

Implication for Vesicle Fusion Mechanism by Alternative, Structural Transformation Model. Past research by Kasemo and co-workers[4,5] experimentally demonstrated the two-step kinetics of vesicle fusion on hydrophilic SiO_x substrates using the QCM-D technique and laid the groundwork for future studies on the vesicle fusion mechanism. Kasemo's proposed mechanism revealed a few important considerations: (1) A critical coverage of vesicles is essential for fusion on hydrophilic substrates. The need for critical vesicle coverage suggests that the interaction between vesicles is necessary for vesicle rupture as shown in Figure 8 (S1). Atomic force microscopy (AFM) by other research groups has demonstrated that, below this critical surface coverage value, adsorbed vesicles remain intact and do

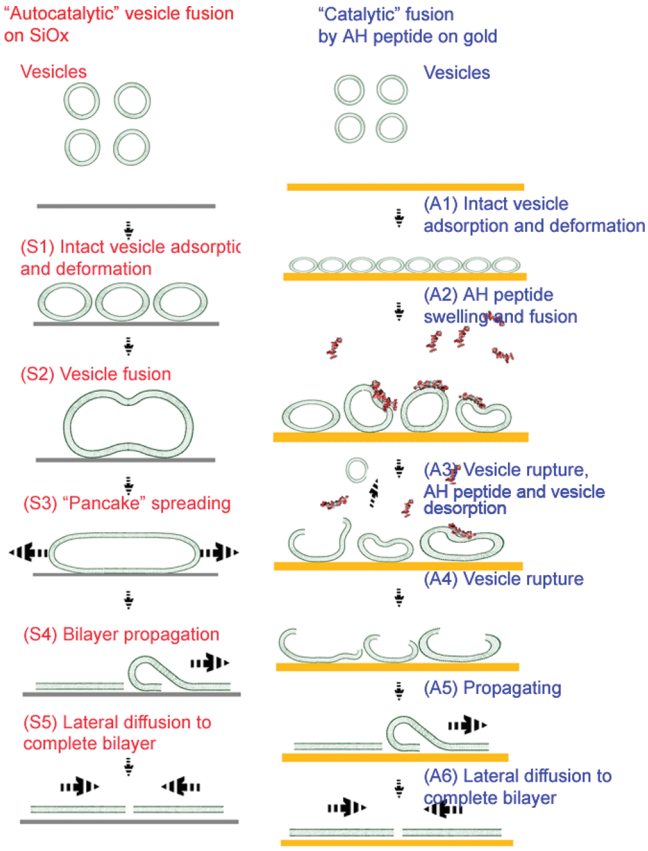

Figure 8. Possible mechanism of "autocatalytic" vesicle fusion on SiO_x and "catalytic" vesicle fusion by AH peptide on gold substrate. (a) (S1) Vesicles diffuse from the bulk to start to adsorb onto the hydrophilic surface, where it continues until reaching a critical concentration of intact vesicles. Vesicle−vesicle interactions cause the adsorbed vesicles to deform and have a more ellipsoidal shape. (S2) After reaching the critical concentration, fusion occurs to form larger vesicles. (S3) Consequently, favorable vesicle−substrate attractions cause the large, intact vesicles to become more ellipsoidal, rupture, and begin to spread on the surface. (S4) Adsorbed bilayer fragments propagate the formation of pores on unruptured vesicles. (S5) The process is completed by the lateral diffusion of bilayer fragments to minimize the number of hydrophobic edges. (b) (A1) Vesicles diffuse from the bulk to make a monolayer of intact vesicles on gold. (A2) AH peptide first binds, leading to vesicle swelling and possibly some fusion events. (A3) Vesicles start to rupture due to swelling and form fingerlike structures on their surfaces. This stage results in the desorption of AH peptide and some lipids and/or vesicles. (A4) Partially ruptured vesicles begin to spread on surface, analogous to "autocatalytic" vesicle fusion. (A5) Similar to (S4). (A6) Similar to (S5).

not rupture.[48] (2) Although a critical coverage is needed, strong attraction between the vesicles and the substrate is also necessary for vesicle rupture. Utilizing several different solid substrates, such as gold and titanium dioxide, researchers have identified that polarizability[4,5] and the isoelectric point are important parameters governing the strength of the van der Waals and electrostatic interactions between vesicles and the aforementioned substrate. Experimental results support that only a few substrates such as SiO_2, mica, and glass are suitable materials to form bilayers from single component zwitterionic phosphatidylcholine (PC) vesicles.[2] Despite being highly polarizable, gold and titanium dioxide substrates do not induce vesicle rupture but rather vesicle adsorption.[5]

AH peptide can be utilized as a "catalyst" to destabilize the vesicle structure. In the absence of AH peptide, this intermediate, destabilized vesicle stage poses an energy barrier preventing the vesicle-to-bilayer transformation. However, the AH peptide−vesicle electrostatic interaction provides the energy to overcome the barrier that normally prevents the vesicle-to-bilayer transformation process on gold by destabilizing the vesicle structure, inducing vesicle swelling and subsequent rupturing. By studying vesicle rupture events induced by different means (surface interactions vs AH peptide as a "catalyst"), we sought to identify a possible mechanism for vesicle rupture on solid supports using the newly defined hydration signature (Figure 6), as illustrated in Figure 8. Following addition of the vesicle solution to the silicon oxide substrate, vesicle adsorption is indicated by a decrease in hydration (Figure 6, red step 1). As the local concentration of adsorbed vesicles reaches the critical value, the vesicle−vesicle and vesicle−substrate interactions are maximized, which has also been shown experimentally by atomic force microscopy (AFM).[31,32] This critical concentration is the point where vesicles reach their maximum deformation (Figure 8 (S2)) and local curvature, inducing pore formation to fuse to bigger vesicles (Figure 8 (S3)). The ruptured bilayer leaflet begins to spread outward along the substrate (Figure 8 (S4)). The resulting thermodynamic instability (hydrophobic edge) propagates expansion of the supported bilayer by promoting the formation of pores on adjacent vesicles and vesicles arriving from solution, as evidenced by a sharp decrease in both the hydration signature (red step 2) and the optical mass (from loss of encapsulated solvent inside vesicles). The propagation continues until the hydrophobic edge is minimized, which is theoretically reached when the bilayer covers the entire substrate space (Figure 8 (S5)). At this point, the vesicle fusion process is complete and a "rigid," nonviscoelastic bilayer exists, as indicated by the hydration signature, which shows that the solvent mass is less than 20% of the acoustic mass.

Similar to bilayer formation on hydrophilic substrates such as silicon oxide, the vesicle adsorption first occurs on gold as shown in Figure 5 and the proposed mechanism in Figure 8 (A1). The slope of the hydration signature is essentially identical to the case of hydrophilic substrates (Figure 6, blue step 1). The absence of strong, attractive electrostatic interactions between the vesicles and the substrate, as in the case of silicon oxide, leads to saturation of the substrate with intact, nonruptured vesicles (~1280 ng cm^{-2}, optical mass of saturated, intact vesicles compared with ~430 ng cm^{-2} for critical vesicle concentration immediately before rupture). Note that the mass change corresponding to maximum, intact vesicle saturation depends on size, concentration, and flow rate. Strikingly, upon injection of AH peptide, the hydration signature rapidly increases from ~80% to ~90% (Figure 6), indicating vesicle swelling (blue step 2, Figure 8 (A3)). In this case, instead of pore formation due to attractive interactions between vesicles and the surface, the AH peptide "catalyzes" pore formation and fusion to form bigger vesicles (Figure 8 (A4)). Once one large vesicle is ruptured by AH peptide, neighboring vesicles rupture in analogous fashion with the "autocatalytic" process observed on SiO_x, as shown in Figure 8b. Most likely, lateral vesicle−vesicle interactions induced upon vesicle swelling also

(48) Schonherr, H.; Rozkiewicz, D. I.; Vancso, G. J. *Langmuir* **2004**, *20*, 7308–7312.

contribute to the rupturing process. Over the course of the 15 min following injection of AH peptide, there is a significant amount of optical mass lost because of desorbing AH peptide and vesicles/lipids, even though the vesicle swelling process continues.

The AH peptide−vesicle interaction raises questions regarding the composition of the supported bilayer formed, particularly whether any AH peptide remains in the supported bilayer. We have shown previously that AH peptide binds to a proteineous component and not to bare lipid molecules,[6] which supports our finding that AH peptides do not bind to a solid-supported bilayer to any appreciable extent (~1 Hz).[6] However, AH peptide binds significantly (~15.8 Hz shift in $\Delta f_z/z$) to an intact vesicle layer prior to the structural transformation. Since AH peptide binds to the vesicle surface, destabilizes the surfaces, and then desorbs, it can be regenerated into its original state and display catalytic behavior. Furthermore, during the vesicle swelling process, vesicle−vesicle interactions may also increase, which could play an important role in the transformation process. Following the vesicle swelling process, the hydration signature's sudden drop represents the loss of encapsulated solvent within vesicles. During this period, the slope of the hydration signature is nearly identical to the bilayer formation on the silicon oxide substrate (Figure 6), demonstrating that the process of vesicle rupture to form a bilayer similarly follows the "autocatalytic" fashion.

For the first time, we have quantitatively examined the "Hit and Run" mechanism that describes the AH peptide's interaction with intact vesicles. When the solvent mass is decoupled from the lipid mass as presented in this paper, it is shown that AH peptide binds to the intact vesicles for ~5 min and then acts as a destabilizing agent toward the intact vesicles, leading to vesicle rupture. Combined QCM-D and reflectometry measurements give new, quantitative insight into the mechanism of the AH peptide−vesicle interaction: (1) The combined technique allowed us to calculate the initial binding mass of AH peptide. (2) The solvent mass increases during the initial vesicle swelling process. (3) Our current study permits us to suggest a general vesicle fusion mechanism by analyzing an alternative structural transformation by AH peptide, which has a nearly identical vesicle rupture process despite a different, initial vesicle adsorption process.

CONCLUSION

In this article, we have presented quantitative insight regarding the structural transformation of intact vesicles to a lipid bilayer on a gold surface induced by the addition of AH peptide, which was resolved by combining QCM-D and reflectometry techniques. Three independently measured physical parameters, resonant frequency shift upon acoustic mass changes on the quartz crystal surface, the damping of the quartz crystal's oscillations, and reflectometry changes due to optical mass change, provide quantitative information that, when collected simultaneously, can lead to a more accurate interpretation of the model system. When the techniques are used separately, misinterpretation of the data is more likely. In addition, from the presented model systems, we were able to quantitatively separate the acoustic and optical masses, which lead to the calculation of the pure solvent mass and the hydration factor of the entire process. Moreover, we were able to present an alternative structural transformation model of the vesicle rupture process caused by AH peptide acting as a destabilizing agent.

With new experimental support, we now have a better mechanistic understanding about the interaction between intact vesicles and AH peptide. First, the AH peptide binds to intact vesicles and destabilizes them. In turn, this promotes vesicle swelling, which leads to heightened vesicle−vesicle interactions and subsequent vesicle rupture. Following the rupturing process, AH peptide does not contribute additional mass to the supported bilayer since it desorbs from the lipid surface. The initial AH peptide−vesicle binding interaction that promotes the catalytic behavior can be modified by adjusting the electrostatic interaction (e.g., lipid composition of the vesicles), vesicle size (line tension of the vesicles), osmotic shock (different buffer conditions inside and outside of vesicles in order to create an osmotic pressure gradient), pH, membrane rigidity (e.g., incorporating cholesterol), or temperature, among many other possibilities. The whole story is complex, however, and considered beyond the scope of the present work. With the complexity of biological interactions, there is a clear need to understand these model systems in order to provide background to understand more complex biomimetic systems. We have demonstrated that it is possible to elucidate the mechanism of complex, biological phenomena by combining multiple, simultaneous measurements of a single process that rely on primarily different physical principles.

ACKNOWLEDGMENT

We acknowledge Dr. K.K. Kanazawa (Consulting Professor, Stanford University) for valuable discussions. N.-J.C. is a recipient of an American Liver Foundation Postdoctoral Fellowship Award and a Stanford Dean's Fellowship. This work was also supported by The International Human Frontier Science Program Organization (HFSP) Postdoctoral Fellowship for N.-J.C.

Received for review February 2, 2009. Accepted March 31, 2009.

AC900242S